JOINT EUROPEAN TORUS JET

JET–P(93)78

I.H. Coffey, R. Bamsley, F.P. Keenan, N.J. Peacock

Ne IX and Ne X Spectra on the JET Tokamak

Neutron Emission Profile Measurements during the First Tritium Experiments at JET

I.H. Coffey[1], R. Bamsley, F.P. Keenan[1], N.J. Peacock[2]

JET-Joint Undertaking, Culham Science Centre, OX14 3DB, Abingdon, UK

[1]Department of Pure and Applied Physics, Queens University, Belfast, BT7 INN, Northern Ireland.
[2]Culham Laboratory, Abingdon, Oxon, OX14 3DB, England.

Preprint of a paper to be submitted for publication in
J. Phys. B.
October 1993

ABSTRACT

Observations of H-like Ne X and He-like Ne IX soft X-ray emission line spectra have been made on the JET (Joint European Torus) tokamak. Recently calculated electron impact excitation rates for He-like neon are used in the derivation of the electron temperature sensitive line ratios $G = [(x + y + z)/w]$, $R_1 = (1s3p\,^1P_1 \rightarrow 1s^2\,^1S_0)/w$, Ly_α/w, and the electron density sensitive ratio $R = [z/(x + y)]$, where w, x, y and z are the resonance line $(1s2p\,^1P_1 \rightarrow 1s^2\,^1S_0)$, intercombination $(1s2p\,^3P_{2,1} \rightarrow 1s^2\,^1S_0)$ and forbidden lines $(1s2s\,^3S_1 \rightarrow 1s^2\,^1S_0)$ respectively and Ly_α is the H-like Lyman_α transition. Extensive modelling is carried out to allow for non-coronal conditions due to diffusion effects in these calculations, which are compared with experimental ratios from JET, where independent temperature and density measurements are available. Departures from equilibrium are found for both ohmic and additionally heated plasmas, resulting in significant changes to the G and Ly_α/w ratios. The R ratio is approaching its upper density limit and is relatively unaffected by non-coronal conditions. Good agreement between the experimental and calculated ratios is found, giving an indication of the accuracy of the combination of atomic data and transport employed in the calculations. This implies that the the theoretical results may be applied to the analysis of remote plasma sources for derivation of these parameters.

INTRODUCTION

Calculations for the $R = [z/(x + y)]$, $G = [(x + y + z)/w]$ and $R_1 = (1s3p\,^1P_1 \rightarrow 1s^2\,^1S_0)/w$ ratios in He-like Ne IX, where w, x, y and z are the resonance line $(1s2p\,^1P_1 \rightarrow 1s^2\,^1S_0)$, intercombination $(1s2p\,^3P_{2,1} \rightarrow 1s^2\,^1S_0)$ and forbidden lines $(1s2s\,^3S_1 \rightarrow 1s^2\,^1S_0)$ respectively, have been presented previously (Keenan *et al.* 1987) for application to temperature and density diagnostics of the solar corona. A comparison with spectra from solar active regions was made, but these suffered from blending with Fe XIX, Fe XVIII and Na X lines. Table 1 gives a comparison between typical temperature and density parameters for the case of the solar corona and solar flares (Phillips, 1991; Dufton and Kingston, 1981) and the JET plasma. The coronal and flare plasmas lie completely within the JET temperature range, whereas only the flare plasma shows an overlap at the lower density edge region of the JET plasma.

In this work comparison is made between experiment and theory for the above ratios on the JET tokamak, where independent radial density and temperature profile measurements are available. A coronal ionisation balance is not assumed as was done

by the above authors, and transport modelling is employed to simulate JET conditions for the line ratio calculations. Experimental H-like to He-like ratios are also measured (ie. the Ne X Ly$_\alpha$ to Ne IX resonance line ratio) using a double crystal monochromator, and compared with theory.

	T_e(eV)	n_e(cm^{-3})
JET Plasma	$10 - 10000$	$10^{12} - 10^{14}$
Solar Corona	$100 - 400$	$10^{8} - 10^{9}$
Solar Flare	$200 - 1700$	$10^{11} - 10^{12}$

Table 1: Comparison of coronal and JET plasma parameters

ATOMIC DATA

Determination of the theoretical line ratios is critically dependent on the atomic data adopted, especially for the electron impact excitation rates between the ground state and the $n = 2$ and 3 levels. In this section details of the atomic models and data sources are given for calculations involving H-like and He-like neon.

For calculations concerning H-like Ne X the atomic model was constructed by interpolation between H I isoelectronic sequence data (C VI, O VIII, Mg XII, Ar XVIII, Fe XXVI and Mo XLII) in the JET Atomic Data and Analysis Structure (ADAS) of Summers *et al.* (1993). The Ne X model comprises the 15 lowest states with $n < 6$ and $l < 6$.

The model ion for Ne IX consisted of the 23 lowest $1snl$ states with $n < 6$ and $l < 3$, making a total of 37 levels when the fine-structure splitting in the ^3P and ^3D terms is included. Energies of the ionic levels are taken from Accad *et al.* (1971), Baskin and Stoner (1975) and Godefroid and Verhaegen (1980).

Electron impact excitation rates for transitions from the ground state to the $1s2l$ and $1s3l$ levels were taken from Keenan *et al.* (1986), and those between $n = 2$ states from Pradhan *et al.* (1981). Rates for transitions to or between higher levels were either derived from the above in conjunction with the n^{-3} scaling law (Gabriel and Heddle 1960) or taken from Sampson *et al.* (1983).

Einstein $\mathcal{A}$-coefficients for transitions from the $n = 2$ and 3 levels were taken from

Schiff *et al.* (1971), Jacobs (1972) and Lin *et al.* (1977), except for the intercombination lines $1s2p\,^3P_1 \rightarrow 1s^2\,^1S_0$ and $1s3p\,^3P_1 \rightarrow 1s^2\,^1S_0$ and the two-photon decay $1s2s\,^1S_0 \rightarrow 1s^2\,^1S_0$, where the results of Laughlin (1978) and Drake *et al.* (1969), respectively were adopted. All other radiative rates were obtained from either Schiff *et al.* (1971) or Cohen and McEachran (1972). The effect of dielectronic and radiative recombination of H-like Ne X on the Ne IX level populations was included by using the recombination coefficients of Mewe and Schrijver (1978) in conjunction with the ionisation balance calculations of Arnaud and Rothenflug (1985).

TRANSPORT MODELLING ON JET

In order to simulate the effect of the JET plasma conditions on the calculated ratios and to determine the radial positions of maximum Ne IX and Ne X emissivity (and hence obtain an estimate of the temperature and density conditions at these positions from the JET diagnostic systems) the SANC0 1-D radial transport code was utilised (Lauro-Taroni, 1993). SANC0 calculates radial profiles of intensity, density and radiated power for all the ionisation stages of a particular impurity element at a given time during a discharge. It takes as its input various parameters generated by the JET diagnostics for each discharge, the relevant atomic data needed to calculate the radial ionisation shell distribution and intensity profiles (ionisation and recombination coefficients etc.), and a set of user-defined parameters describing radial impurity transport and an impurity source function.

An important factor in modelling impurity behaviour is the transport coefficients used. For this work radially dependent transport diffusion and inward convective velocity coefficients $D(\mathrm{m^2s^{-1}})$ and $V(\mathrm{ms^{-2}})$ were taken from Pasini *et al.* (1990, 1991). These coefficients were derived using the laser blow-off system on JET (Magyar *et al.* 1989), by simulating the soft X-ray emissivity profiles of impurities introduced into the plasma by this method using an imprity transport code. The values of D and V thus derived are $1\mathrm{m^2s^{-1}}$ and $2\mathrm{ms^{-1}}$ for ohmic plasmas and $3\mathrm{m^2s^{-1}}$ and $6\mathrm{ms^{-1}}$ for additionally heated plasmas respectively at the radial emission position of Ne IX and Ne X.

In order to investigate the behaviour of individual lines a code was developed to utilise the SANC0 outputs of radial distribution of electron temperature and density and impurity densities as inputs to the ADAS statistical balance population code. This enabled a more complex atomic model to be used in derivation of the various line intensities (such

as that described in the previous chapter) than is employed by the SANC0 code (an approximate approach to the line intensities is taken in SANC0 to reduce CPU time). This code is specifically designed to model the emission of the H-like, He-like and Li-like systems for arbitrary departures from coronal ionisation balance (the actual ionisation balance between these three stages is provided by SANC0). Typical radial intensity profiles for the Ne IX emission lines w, x, y and z are shown in figure 1 together with the SANC0 generated w line.

DOUBLE CRYSTAL MONOCHROMATOR MEASUREMENTS ON JET

Neon was introduced into the JET plasma by gas puffing over a series of discharges. The JET device (Rebut *et al.*, 1987) has major and minor radii of 2.96m and 1.25m respectively, a maximum toroidal field of 3.45T and a maximum toroidal current of 7MA. Typical central electron densities and temperatures considered are $n_e \simeq 2.5 \times 10^{13}\text{cm}^{-3}$ and $T_e \simeq 2.5\text{keV}$ respectively. The spectra were obtained with a double crystal X-ray monochromator (Barnsley *et al.*, 1992), which was situated outside the biological shield of the torus hall for maximum shielding from neutrons and hard X-rays. It was used in general survey mode, with a TLAP crystal ($2d = 2.576\text{nm}$) providing coverage of the wavelength region from 1.13nm to 2.24nm, with a resolving power ($\lambda/\delta\lambda$) of $\simeq 500$. The detector was a multiwire proportional counter which could operate at 10MHz. The radial position of maximum emissivity for Ne IX was obtained using the SANC0 transport code mentioned previously. Radial profiles of electron temperature and density were measured by analysis of Electron Cyclotron Emission (Costley 1982) and far infrared interferometry (Orlinski and Magyar, 1988) respectively, or by Thomson scattering of a ruby laser (Salzmann *et al.* 1985) for both quantities.

Figure 2 shows an example of the neon spectra obtained. In addition to the w, x, y and z lines (at 1.3447nm, 1.3550nm, 1.3553 and 1.370nm respectively), the Ne X Ly_α line at 1.2132nm and the Ne IX $n = 3$ resonance line at 1.1554nm are also visible. Contributions from unresolved Li-like satellites to the He-like system were estimated as a fraction of the resonance line using the data of Nilsen (1988) and that outlined above. No exact blends were found, and these calculations showed that the maximum satellite line intensities were $< 5\%$ of the resonance intensity for plasma conditions expected on JET, and hence their contributions were neglected. The satellites will become significant for heavier atoms as the satellite to resonance ratio increases with Z, mainly due to the Z^4 scaling of the radiative transition rates.

RESULTS

Using the ADAS statistical balance population code in conjunction with the atomic data discussed above, ionisation equilibrium Ne IX and Ne X excited state populations were calculated for a range of electron temperatures and densities. Photo-excitation and de-excitation processes are negligible in comparison with the corresponding collisional processes and all transitions were considered optically thin. From these populations various diagnostic line ratios were calculated.

The temperature sensitive G ratio is plotted in figure 3. Recombination into the triplet states results in the flattening of the theoretical curve as T_e increases (Pradhan and Shull, 1981). The model calculations assume ionisation equilibrium where there is a balance between the various ionisation and recombination processes and transport effects are absent. This generally valid in the centre of a tokamak, although the Ne IX emission shell is located close to the edge of the plasma in JET. A diffusive ionisation model calculated using the transport code produces the curve also shown in figure 3 and is in good agreement with experimental values.

To allow for the effect of averaging over the line-of -sight of the spectrometer, these calculated ratios were integrated over the line-of-sight temperature and density profiles. These are plotted at temperatures measured at the calculated radial position of peak emissivity. The emission profiles are generally quite narrow (see figure 6) and the difference between the integrated ratios and those calculated for a single temperature at the emissivity peak ranges between 5% and 15%.

Table 2 gives the comparison between the theoretical G ratios calculated for equilibrium and diffusive ionisation balances and the measured ratios, as well as the ionisation balances used in the calculations. The equilibrium balance calculations are obtained by setting the D and V parameters to zero when using the SANC0 code. Experimentally measured temperatures at the corresponding emissivity peaks are also shown. The average difference between the experimental values and the theoretical G ratio calculated for JET conditions is typically 10%. The N_H/N_{He} ratios are lower for JET conditions than they would be in the non-diffusive case. In effect the Ne IX is in an ionising situation and is occurring at temperatures significantly greater than its temperature of maximum emissivity, $T_m \simeq 310$eV in equilibrium (Gabriel, 1972), as a result of inward diffusion. The SANC0 diffusive balance calculations predict a radial emissivity peak po-

Shot (scan)	T_e(eV) (measured, coronal)	G_{cor} (calculated, coronal)	T_e(eV) (measured, diffusive)	G_{diff} (calculated, diffusive)	G_{exp} (measured)	N_H/N_{He} (calculated, coronal)	N_H/N_{He} (calculated, diffusive)
25818(3)	353	0.825	705	0.462	0.477	6.560	1.069
25818(4)	582	0.658	856	0.441	0.456	7.351	1.146
25818(5)	300	0.865	829	0.351	0.343	8.614	1.327
25819(3)	485	0.689	574	0.448	0.565	3.801	1.126
25819(4)	363	0.814	732	0.507	0.516	5.720	0.950
25819(5)	287	0.875	773	0.534	0.468	7.743	1.298
25820(4)	278	0.932	696	0.540	0.476	6.425	1.012
25820(5)	290	0.865	789	0.552	0.498	7.886	1.235
25821(4)	280	0.765	575	0.521	0.585	3.801	1.427
25821(5)	257	0.746	498	0.551	0.602	2.715	1.356
25823(5)	291	0.764	505	0.660	0.564	2.930	1.947
25823(6)	296	0.756	520	0.650	0.720	2.189	1.202

Table 2: Ne IX G ratios on JET. Column 1 gives the JET shot-number, with the spectrometer scan number in brackets. In column 2 the measured temperature at the calculated radius of peak emissivity of the resonance line for each shot(scan) is given for a coronal ionisation balance, with the corresponding calculated G ratios in column 3. Columns 4 and 5 are equivalent to columns two and three, except that a SANCO generated diffusive ionisation balance is used in the calculations. The measured ratios for each shot(scan) are shown in column 6. Columns 7 and 8 contain the N_H/N_{He} ratios at the radial emissivity peak positions for the coronal and diffusive cases respectively

sition up to 20cm closer to the plasma centre than that calculated for coronal conditions (see figure 6). The calculated temperature difference between the two cases varies from approximately 100 to 500eV depending on such parameters as the D and V profiles used and the temperature and density gradients at the emission radius. In general this temperature difference is greatest during additional heating where these parameters are at their extremes.

Figure 4 shows the density sensitive R ratio. Inclusion of recombination effects increases the R values at low n_e. This increase is small for JET plasma densities, and hence the departure from coronal conditions has little effect. In the low density limit the R ratio (R_0) varies weakly with temperature, changing by a factor of approximately 1.3 over the temperature range T_e = 90eV to T_e = 900eV The R ratio varies strongly with n_e between $n_e = 3.2 \times 10^{10}\text{cm}^{-3}$ to $n_e = 3.2 \times 10^{12}\text{cm}^{-3}$, which is again relevant to solar diagnostics. The JET experimental points lie in the density range $n_e = 6.3 \times 10^{12}\text{cm}^{-3}$ to $n_e = 3.2 \times 10^{13}\text{cm}^{-3}$, which is outside the coronal interest region, but are in good agreement with theory over these densities.

In figure 5 the temperature sensitive ratio R_1 is plotted. Due to the spectral separation of the lines in this ratio the wavelength calibration of the TLAP crystal was required, and the measurements of Christiansen (1991) were utilised for this purpose. Recombination is of lesser importance in determining R_1 than for the G ratio. The temperature range T_e = 90eV to T_e = 900eV comprises the range in which the Ne IX ratios are useful as temperature diagnostics for the solar corona.

Table 3 gives the line-of-sight integrated Ly_α/w ratios calculated from these profiles, compared with experimental measurements. Again calculations are given for both the equilibrium and diffusive cases. The equilibrium calculations consistently predict this ratio to be less than unity, whereas the diffusive calculations show much better agreement with the measured ratios. The calculated radial emissivity profiles for H-like and He-like neon given in figure 6 show that for a equilibrium situation the emission shells are narrow and located at approximately the same radius. The diffusive calculations predict broader profiles which are positioned closer to the centre of the plasma and hence at higher temperatures. This has the effect of increasing the H-like emission relative to the He-like case, thus increasing the observed ratio. Also the He-like ion is occurring at temperatures in excess of T_m causing a reduction in the predicted coronal N_H/N_{He} ratio at such temperatures. The result of this is reduced recombination contributions

Shot(scan)	Ly_α/w (coronal,) calculated)	Ly_α/w (diffusive, calculated)	Ly_α/w (experimental, measured)
25818(4)	1.333	2.230	1.777
25818(5)	0.296	1.530	1.548
25819(4)	0.652	2.103	1.412
25819(5)	0.369	1.984	1.980
25820(4)	0.267	2.170	2.266
25820(5)	0.791	2.178	1.690
25821(4)	0.628	2.204	2.066
25821(5)	0.559	2.135	1.859

Table 3: Neon Ly_α/w ratios on JET.Column 1 gives the JET shot-number, with the spectrometer scan number in brackets. Columns 2 and 3 show the calculated Ly_α/w ratios at the radial emissivity peak position for a coronal and a diffusive balance respectively. Column 4 contains the JET measured ratios for each shot(scan)

into the He-like triplet levels as was observed for the G ratio.

Blending with iron emission lines was discounted for the above spectrum as the intensities of unblended iron lines in the surrounding wavelength region was negligible. Previous authors (McKenzie, 1985; Keenan *et al.* 1987 and Bhatia *et al.* 1989) have reported blending to the x and y lines from Fe XIX emission which would increase the apparent density (by decreasing the measured R ratio) and decrease the apparent temperature (by increasing the measured G ratio). In addition a Fe XVIII blend to the $n = 3$ resonance line has been identified, and for solar spectra the $n = 4$ resonance line coincides with the Na X resonance line (sodium has never been observed on JET).

CONCLUSIONS

H-like and He-like neon spectra were observed and the various diagnostic emission line ratios calculated and compared with experimental results from the JET tokamak. The main objective of these neon observations was to test the accuracy of the atomic data/transport model against experimental results obtained under known conditions. He-like neon diagnostic ratios are density and temperature sensitive in regions applicable to diagnostics of the solar corona and solar flares, and hence comparison of the calculated ratios with those from a well diagnosed plasma such as JET is desirable.

Extensive modelling of the JET plasma conditions using the SANC0 transport code in conjunction with the ADAS statistical balance population codes (where independent measurements of n_e and T_e were available as inputs to these codes) was carried out. Line-of-sight integrated calculations of the R, G, R_1 and Ly_α/w ratios derived from these codes proved to be in good agreement with the measured values, providing support for the combination of atomic data and the transport model utilised.

Due to the high central electron temperature of the JET device compared to the temperature of maximum emissivity II-like and He-like neon, the neon emission shells were predicted to be located close to the plasma edge. In this region the steep temperature and density gradients pointed to a departure from ionisation equilibrium conditions, and a diffusive ionisation balance calculated from the SANC0 code proved to give much better agreement with experiment than the equilibrium model calculation.

In general the neon emission shells were located at temperatures in excess of their coronal counterpart, and were in an ionising situation. For the H-like and He-like stages this resulted in a reduced N_H/N_{He} ratio, and hence reduced population of the He-like triplet levels by recombination into the H-like ionisation stage. The G ratio was affected in particular, being significantly reduced from its coronal value at the measured temperatures. The Ly_α/w ratio was also affected by these conditions, with the diffusive calculations giving ratios up to four times greater than the equivalent coronal result. In contrast the R_1 ratio is largely unaffected by recombination, and so was not as dependent upon the accuracy of the modelling for comparison with experiment. Results over the temperature range 500eV – 850eV were obtained with good agreement between theory and experiment. This temperature range is particularly relevant to solar flare diagnostics, although results in the 100eV – 400eV would be desirable for comparison with spectra obtained from the solar corona.

For the R ratio, conditions on JET were at the upper extreme of the density sensitive region. The measured ratios were in reasonable agreement with theory, but do not cover a wide enough range to verify the accuracy of the ratio in the density range 10^8–$10^{12}\mathrm{cm}^{-3}$ which would be applicable to diagnostics of the solar corona and solar flares.

In summary the agreement between the calculated and measured ratios for JET gives a

good indication of the accuracy of the combination of atomic data and transport model used. The use of these ratios for remote plasma measurements has been successfully demonstrated over the T_e and n_e range described above, and lend s support to their usage as solar diagnostics. In particular the detection of non-equilibrium conditions is applicable to the impulsive phase of solar flares.

ACKNOWLEDGEMENTS

We would like to thank Professor A. E. Kingston, Dr. P. R. Thomas and Dr. R. Giannella for their interest in the work, to L. Lauro-Taroni for use of the SANC0 code, and to Professor H. P. Summers and W J. Dickson for the use of the ADAS codes. IHC is grateful to the Culham laboratory for financial support. Thc authors are indebted to the staff involved at the JET and Culham laboratories.

BIBLIOGRAPHY

Accad Y, Perkeris C L and Schiff B, 1971 *Phys. Rev.* A **4**, 516

Arnaud M. and Rothenflug R 1985 *Astr. Ap. Suppl.* **60** 425

Barnsley R, Schumacher U, Källne E, Morsi H W and Rupprecht G 1992 *Rev. Sci. Instrum.* **62** 889

Bashkin S and Stoner S O 1975 *Atomic Energy Levels and Grotrian Diagrams, Amsterdam:North Holland*

Bhatia A K, Fawcett B C, Lemen J R, Mason, H E and Phillips K J H 1989 *Mon. Not. R. Astr. Soc.* **240** 421

Christiansen H. 1991 *MSc. Thesis, Royal Institute of Technology, Sweden*

Cohen M and McEachran R P 1972 *Canadian J. Phys.* **50** 1363

Costley A 1982 *Diagnostics for Fusion Reactor Conditions, EUR 83 51-1 En. Commission of the European Communities Brussels* 129

Drake G W F, Victor G A and Dalgarno A 1969 *Phys. Rev.* **180** 25

Dufton P L and Kingston A E 1981 *Adv. Atomic. Molec. Physics* **17** 355

Gabriel A H 1972 *Mon. Not. R. Astron. Soc.* **160** 99

Gabriel A H and Heddle D W 1960 *Proc. Roy. Soc. London* A **258** 124

Godefroid M and Verhaegen G 1980 *J. Phys.* B **13** 3081

Jacobs V L 1972 *J. Phys.* B **5** 213

Keenan F P, Kingston A E and McKenzie D L 1986 *Ap. J.* **303** 486

Keenan F P, McKenzie D L, McCann S M and Kingston A E 1987 *Ap. J.* **318** 926

Laughlin C 1978 *J. Phys.* B **11** L391

Lauro-Taroni L 1993 *JET Laboratory, private communication*

Lin C D, Johnston W R and Dalgarno A 1977 *Phys. Rev.* A **15** 154

Magyar G, Barnes M, Edwards A W *et al* 1988 *JET Report* JET-R(88)15

McKenzie D L 1985 *Ap. J.* **296** 294

Mewe R and Schrijver J 1978 *Astr. Ap.* **65** 99

Nilsen J 1988 *At. Data. Nucl. Data Tables* **38** 339

Orlinski D V and Magyar G 1988 *Nucl. Fusion* **29** 611

Pasini D, Mattioli M, Edwards A *et. al.* 1990 *Nucl. Fusion* **30** 2049

Pasini D, Giannella R, Lauro-Taroni L, Mattioli M, Denne-Hinnov B, Hawkes N, Magyar G and Weise H 1991 *Plasma Physics and Controlled Fusion* **34** 677

Philipps K J H 1991 *Phil. Trans. R. Soc. Lond.* A **336** 461

Pradhan A K and Shull J M 1981 *Astrophys. J.* **249** 821

Pradhan A K, Norcross D W and Hummer D G 1981 *Ap. J.* **246** 1031

Rebut P H *et al.* 1987 *Fus. Tech.* **11** 11 Vol.1
Salzmann H, Hirsch K, Rohr J, Bredow G and Witte K 1985 *Rev. Sci. Inst.* **56** 1030
Sampson D H, Goett S J and Clark R E 1983 *Atomic Data and Nucl. Data Tables* **29** 467
Schiff B, Perkeris C L and Accad Y 1971 *Phys. Rev.* A **4** 885
Summers H P, Briden P, Dickson W J and Lang J. 1993 *An Atomic Data and Analysis Structure for Spectral Emission in Laboratory and Astrophysical Plasmas*- In preparation

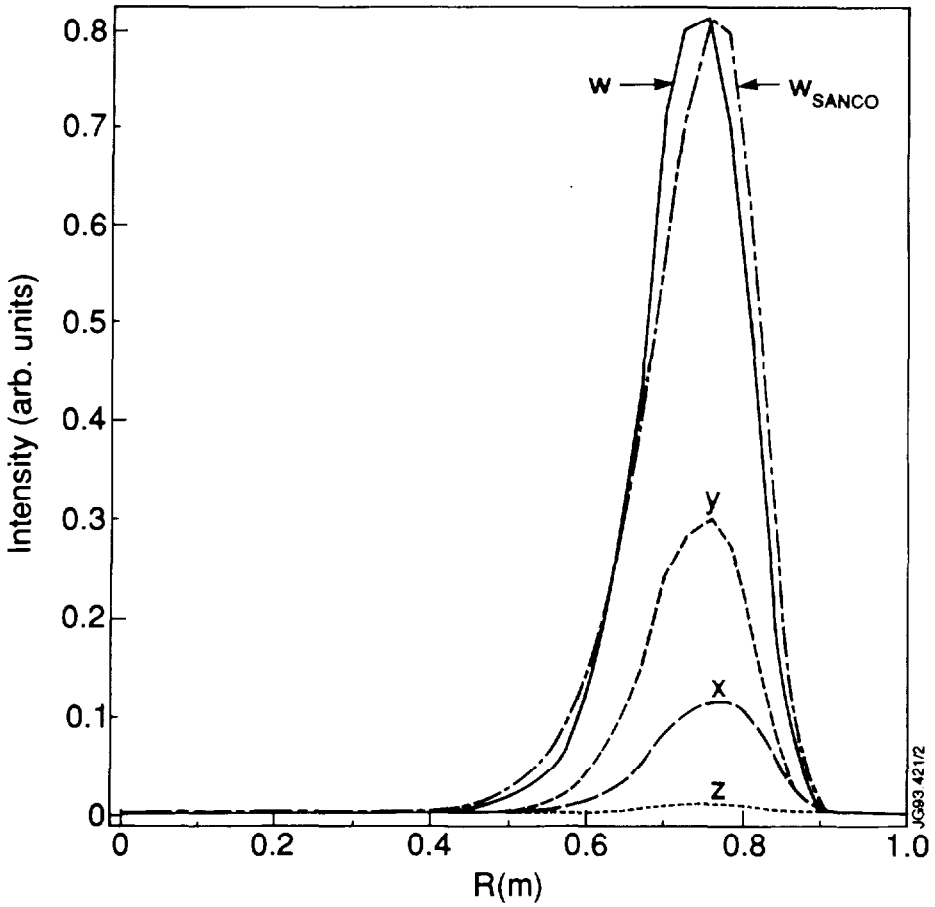

Figure 1. Radial intensity profiles for the Ne IX emission lines w ($1s2p\,^1P_1 \rightarrow 1s^2\,^1S_0$), x,y ($1s2p\,^3P_{2,1} \rightarrow 1s^2\,^1S_0$ respectively) and z ($1s2s\,^3S_1 \rightarrow 1s^2\,^1S_0$), calculated using the ADAS statistical balance population code in conjunction with a diffusive ionisation balance provided by the SANC0 code (JET pulse:25818). Also shown is the equivalent w line profile generated by the SANC0 code alone.

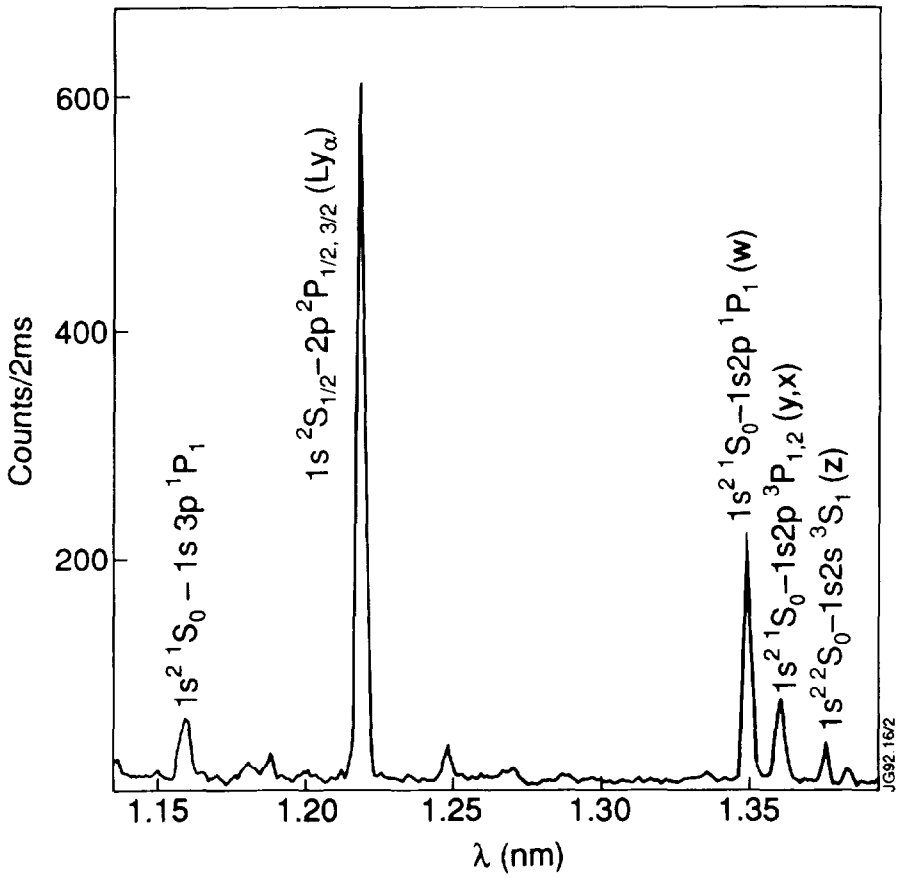

Figure 2. Measured spectrum of H-like Ne X and He-like Ne IX neon from JET (JET pulse:25818).

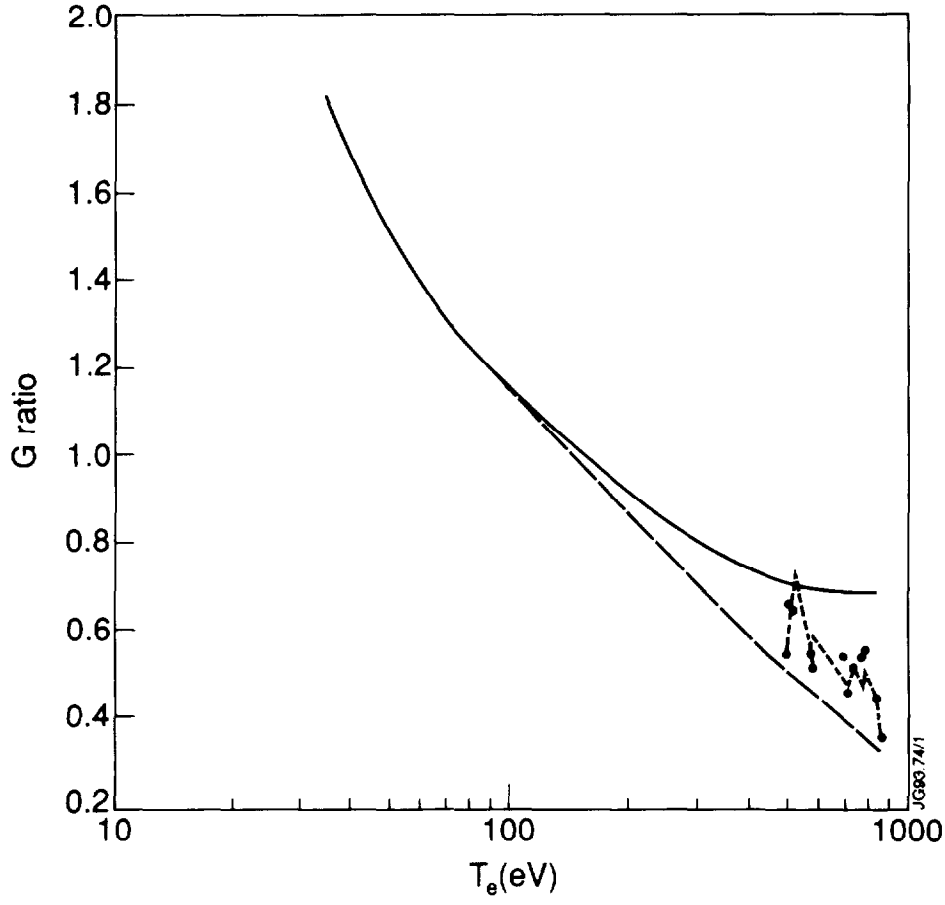

Figure 3. The Theoretical emission ratio G plotted as a function of temperature T_e (eV) at an electron density of $n_e = 1 \times 10^{13}\text{cm}^{-3}$, with dielectronic and radiative recombination included in (solid line) or excluded from (long dashed line) the calculations. Also shown is the theoretical G ratio (short dashed line) calculated using an ionisation balance calculated for JET plasma conditions at each of the experimental results (solid points). Typical errors in the JET experimental data, which are measured at densities ranging from $n_e = 6.3 \times 10^{12}\text{cm}^{-3}$ to $n_e = 3.2 \times 10^{13}\text{cm}^{-3}$, are $\pm 10.0\%$ in G_{obs} and $\pm 15\%$ in T_e.

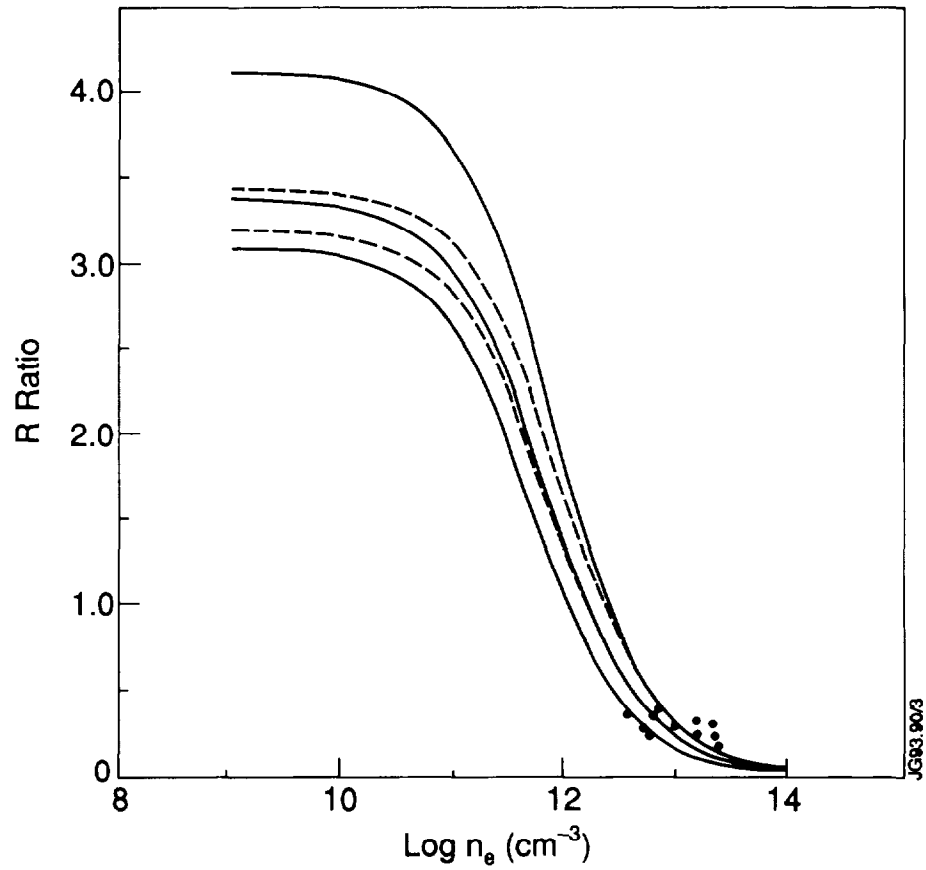

Figure 4. The theoretical emission ratio R plotted as a function of density n_e, at electron temperatures (top to bottom), T_e =900, 340 and 90eV, with dielectronic and radiative recombination included (solid lines) or excluded (dashed lines). Also shown are the measured values from JET (solid points) which have an average electron temperature of $T_e \simeq$ 620eV. Errors in the JET experimental data are $\pm$10.0% in R_{obs} and $\pm$13.0% in n_e.

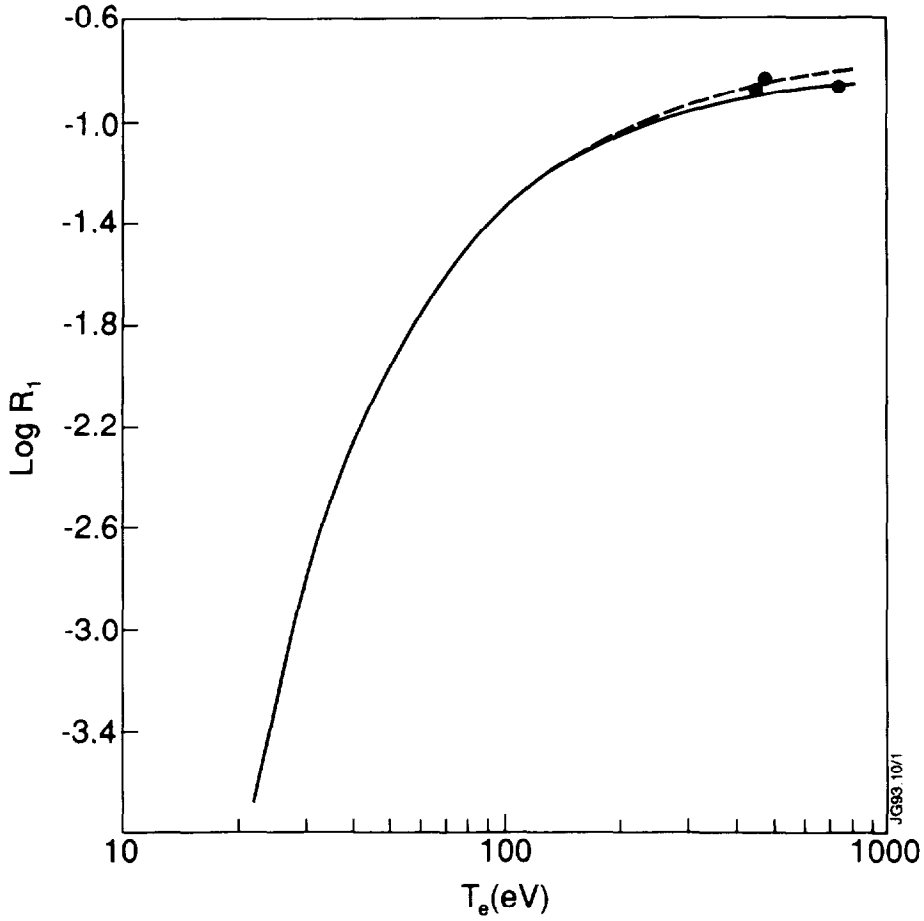

Figure 5. The theoretical emission ratio R_1 plotted as a function of temperature T_e with dielectronic and radiative recombination included (solid line) or excluded (dashed line). Typical errors in the measured values from JET (solid points) are $\pm 10.0\%$ in R_{1obs} and $\pm 15.0\%$ in T_e.

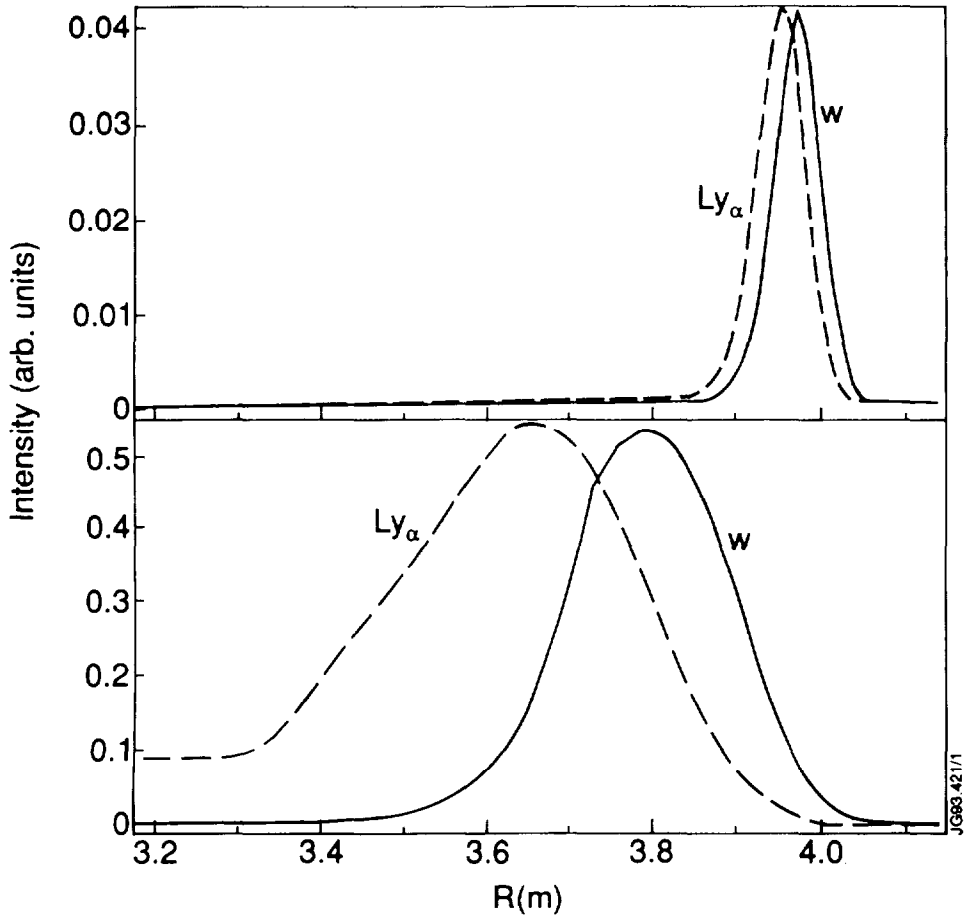

Figure 6. Calculated radial emissivity profiles (arbitrary units for the Ne IX w line (solid line) and the Ne X Ly$_\alpha$ line (dashed line). Profiles are given for a coronal ionisation balance (top) and a diffusive balance calculated by the SANC0 code (bottom). Both sets of calculations were performed for the same input temperature and density profiles (JET pulse:25818).